# Zeroth-Order Flutter Prediction for Cantilevered Plates in Supersonic Flow

Marius-Corné Meijer[a,*], Laurent Dala[a,b]

[a]*Department of Mechanical and Aeronautical Engineering, University of Pretoria, Pretoria, 0028, South Africa*
[b]*CSIR, DPSS Aeronautic Systems, Pretoria, 0001, South Africa*

**Abstract**

An aeroelastic prediction framework in MATLAB with modularity in the quasi-steady aerodynamic methodology is developed. Local piston theory (LPT) is integrated with quasi-steady methods including shock-expansion theory and the Supersonic Hypersonic Arbitrary Body Program (SHABP) as a computationally inexpensive aerodynamic solver. Structural analysis is performed using bilinear Mindlin-Reissner quadrilateral plate elements. Strong coupling of the full-order system and linearization of the modal-order system are implemented. The methodology is validated against published experimental data in literature and benchmarked against Euler computation in the Edge CFD code. The flutter dynamic pressure is predicted to within 10% of the experimental value for 140 times lower computational cost compared to CFD. Good agreement in other cases is obtained with the industry-standard ZONA7 and ZONA7U codes.

*Keywords:* zeroth-order, flutter, local piston theory, shock-expansion, cantilevered plate

## 1. Introduction

The modeling of multiphysics phenomena such aeroelasticity in the preliminary design of aerospace components is important in reducing the risk of the design not meeting requirements for structural integrity and safety. Typically, the prohibitive computational cost of multidisciplinary analysis results in such studies only being conducted in the detailed design phase. The reduction of the computational cost of aeroelastic prediction would allow for such analysis to be conducted earlier in the design cycle, and would allow for better filtering of concepts in the design space.

Modeling of the multiphysics problem is most broadly done through the use of segregated solvers — the equations for the structural dynamics and aerodynamic loading are solved separately. The exchange of data between the solvers is referred to as coupling. Strong coupling of the solvers refers to the practice of performing multiple iterations of data exchange between the solvers per time-step in the solution, in order to achieve dynamic equilibrium; weak coupling of the solvers disregards this subiteration, and only one exchange of data between solvers is performed per time-step. Early work in computational aeroelasticity (Rodden et al., 1962a,b) involved the use of monolithic solvers, in which the structural dynamics and aerodynamics are computed simultaneously. This work was associated with matrix (panel) methods. The aerodynamic models employed in such methods are typically applicable to both steady and unsteady flows. However, these aerodynamic models may also be exploited in segregated aeroelastic solvers, with coupling to a finite-element structural model; an example of this would be to use the Supersonic/Hypersonic Arbitrary Body Program (SHABP) code (Gentry et al., 1973) (which is modular in the quasi-steady aerodynamic methods used) to provide the loading for a structural model derived from the finite-element method (FEM).

The advantage offered by the use of the aforementioned approximate aerodynamic methods is the significantly lower computational cost of the methods compared to high-fidelity aerodynamic analysis by computational fluid dynamics (CFD). The use of computationally inexpensive approximate methods in computational aeroelasticity continues (Yurkovich, 2003) alongside high-fidelity analysis involving the coupling of computational structural dynamics (CSD) and CFD solvers (Livne, 2003; McNamara and Friedmann, 2011). The ability of approximate methods to

*Corresponding author.
*Email addresses:* mariuscmeijer@gmail.com (Marius-Corné Meijer), ldala1@csir.co.za (Laurent Dala)

reproduce aerodynamic and aeroelastic trends for significantly lower computational cost (compared to CSD-CFD solutions) renders them valuable in guiding higher-fidelity analysis, and makes multidisciplinary design feasible in the preliminary design cycle.

To this end, the current work suggests a computationally inexpensive framework for flutter prediction through the use of approximate aerodynamic modeling. The framework offers modularity in the quasi-steady aerodynamic methods employed, using local piston theory to compute the unsteady aerodynamic contribution. This allows for consistent comparison of the merits of various approximate quasi-steady models for flutter analysis. The purpose of the work is thus to provide the designer with a method to rapidly model the aeroelastic response of a concept, in order to filter through the design space, and to provide the guiding "zeroth-order" solution upon which increasingly higher-fidelity analysis improves.

## 2. Modeling Methodology

### *2.1. Structural Dynamics*

#### *2.1.1. Structural Model*

A structural solver was developed in MATLAB as a core component of the computational framework. A finite-element structural model based on Mindlin-Reissner plate theory (Ferreira, 2008) was implemented for thin plates ($t/c \leq 0.1$) of trapezoidal planform. Bilinear quadrilateral plate elements with varying thickness were employed. The spanwise discretization of the planform was in this study restricted to producing successive chordwise sections that were parallel to the cantilevered root; no restriction was made on the chordwise discretization. The plate was modeled as having linear isotropic material properties.

#### *2.1.2. Aeroelastic System*

Two methods were adopted in incorporating the loading on the structural model from the aerodynamic solver: a modal representation with time-invariant linearized generalized aerodynamic forces (GAFs), and a strongly-coupled full-order model.

In the linearized system, a truncated modal representation of the structure was used in linearizing the GAFs from the aerodynamic solver. The GAFs were computed once, about the trim condition, for small increments in modal displacements and velocities. The aeroelastic system is described by Eq. (1).

$$\mathbf{I}\ddot{\mathbf{q}} + \mathbf{D_s}\dot{\mathbf{q}} + \mathbf{\Omega_s}\mathbf{q} = \mathbf{D_a}\dot{\mathbf{q}} + \mathbf{\Omega_a}\mathbf{q} \tag{1}$$

where $\mathbf{I}$ is the identity matrix, $\mathbf{D_s}$ is the modal structural damping matrix, $\mathbf{D_a}$ is the aerodynamic damping matrix, $\mathbf{\Omega_s}$ is the matrix of structural modal frequencies, $\mathbf{\Omega_s}$ is the matrix of aerodynamic modal frequencies, $\mathbf{q}$ are the generalized coordinates, and dot notation denotes derivation with respect to time.

The resulting analysis resulted in a linear time-invariant aeroelastic system of truncated modal order. This allowed for the direct extraction of aeroelastic eigenvalues and for inexpensive computation of the time-history of system response. The aeroelastic modal parameters were used to calculate the Zimmerman-Weissenburger flutter margin as an indication of the stability trends. The two-mode characteristic equation of a continuous-time system has the form (Dimitriadis, 2001):

$$G(\lambda) = \lambda^4 + A_1\lambda^3 + A_2\lambda^2 + A_3\lambda + A_4 \tag{2}$$

where $G(\lambda)$ is the characteristic polynomial of the continuous-time system and the $\lambda$ are the eigenvalues of the system. The associated Zimmerman-Weissenburger flutter margin $F_Z$ of the two modes is given (Dimitriadis, 2001) by:

$$F_Z = A_2\left(\frac{A_1}{A_3}\right) - \left(\frac{A_1}{A_3}\right)^2 + A_0 \tag{3}$$

The strongly-coupled aeroelastic system saw the full-order structural model used to compute the aerodynamic loading. Solution of the system response was obtained through direct integration of the full-order model, which is described by Eq. (4).

$$\mathbf{M}\ddot{\mathbf{x}} + \mathbf{C}\dot{\mathbf{x}} + \mathbf{K}\mathbf{x} = \mathbf{F} \tag{4}$$

where $\mathbf{M}$ is the structural mass matrix, $\mathbf{C}$ is the structural damping matrix, $\mathbf{K}$ is the structural stiffness matrix, $\mathbf{F}$ is the aerodynamic loading vector, and $\mathbf{x}$ is the displacement vector.

The Newmark-$\beta$ time-marching scheme was used with successive updates of the structural response and the aerodynamic loading being performed to convergence at each physical time step ($\Delta t$) to achieve strong coupling. The equations of the scheme are given (Katona et al., 1977) by:

$$\ddot{\mathbf{x}}_{t+\Delta t} = \mathbf{B}^{-1}\left(\mathbf{F}_{t+\Delta t} - \mathbf{C}\tilde{\dot{\mathbf{x}}}_{t+\Delta t} + \mathbf{K}\tilde{\mathbf{x}}_{t+\Delta t}\right) \tag{5}$$

$$\dot{\mathbf{x}}_{t+\Delta t} = \tilde{\dot{\mathbf{x}}}_{t+\Delta t} + (\gamma_S \Delta t)\,\ddot{\mathbf{x}}_{t+\Delta t} \tag{6}$$

$$\mathbf{x}_{t+\Delta t} = \tilde{\mathbf{x}}_{t+\Delta t} + \left(\beta \Delta t^2\right)\ddot{\mathbf{x}}_{t+\Delta t} \tag{7}$$

in which:

$$\mathbf{B} = \mathbf{M} + \gamma_S \Delta t \mathbf{C} + \beta \Delta t^2 \mathbf{K} \tag{8}$$

$$\tilde{\dot{\mathbf{x}}}_{t+\Delta t} = \dot{\mathbf{x}}_t + \Delta t\,(1-\gamma_S)\,\ddot{\mathbf{x}}_t \tag{9}$$

$$\tilde{\mathbf{x}}_{t+\Delta t} = \mathbf{x}_t + \Delta t \dot{\mathbf{x}}_t + \frac{\Delta t^2}{2}\,(1-2\beta)\,\ddot{\mathbf{x}}_t \tag{10}$$

where $\mathbf{x}_t$ is the displacement at time $t$. The parameters $\gamma_S$ and $\beta$ of the Newmark-$\beta$ scheme were chosen as in Eqs. (11, 12) for unconditional stability of the numerical scheme (Katona et al., 1977); the coarsest recommended (Katona et al., 1977) time-step for suitable resolution of the lower-frequency modes being given by Eq. (13).

$$\gamma_S = 1/2 \tag{11}$$

$$\beta = 1/4 \tag{12}$$

$$\Delta t = \frac{T_{min}}{\pi^2} \tag{13}$$

where $T_{min}$ is the shortest period of the truncated mode set. The

Modal parameters were estimated from the time-history of the system response, with the response of the leading-edge and trailing-edge nodes at the tip of the cantilevered plate used in constructing autoregressive moving-average (ARMA) models of the aeroelastic system. The ARMA model for an aeroelastic system may be described (Torii, 2012) by:

$$x_t + \sum_{i=1}^{n} \alpha_i x_{t-i} = e_t + \sum_{i=1}^{m} \epsilon_i e_{t-i} \tag{14}$$

where $x_t$ is the displacement at time $t$, $e_t$ is a white noise signal at time $t$, $\alpha_i$ are the autoregressive coefficients, and $\epsilon$ are the moving-average coefficients. The `armax` function in MATLAB was employed to estimate a 2 DOF model, using a $4^{\text{th}}$-order autoregressive component and a $1^{\text{st}}$-order moving average component, following the approach of McNamara and Friedmann (2007). The ARMA model for a 2 DOF system provides the characteristic equation of the aeroelastic system as:

$$G(Z) = Z^4 + \alpha_1 Z^3 + \alpha_2 Z^2 + \alpha_3 Z + \alpha_4 \tag{15}$$

where $G(Z)$ is the characteristic polynomial of the discrete-time system, with eigenvalues in the form:

$$Z_i = r_i + i s_i \tag{16}$$

The modal damping ratios $\zeta_i$ and modal frequencies $f_i$ were estimated from eigenvalues using the relations (McNamara and Friedmann, 2007):

$$\zeta_i = \frac{1}{2\Delta t} \log_e\left(r_i^2 + s_i^2\right) \tag{17}$$

$$f_i = \frac{1}{2\pi\Delta t} \tan^{-1}\frac{s_i}{r_i} \tag{18}$$

The ARMA-coefficients were subsequently used to compute the flutter margin for discrete systems $F_D$ to estimate the flutter point for the assumed 2 DOF system using (Torii, 2012):

$$F_D = \frac{\det(X_3 - Y_3)}{(1 - \alpha_4)^2} \tag{19}$$

where:

$$X_3 = \begin{pmatrix} 1 & \alpha_1 & \alpha_2 \\ 0 & 1 & \alpha_1 \\ 0 & 0 & 1 \end{pmatrix} \tag{20}$$

$$Y_3 = \begin{pmatrix} \alpha_2 & \alpha_3 & \alpha_4 \\ \alpha_3 & \alpha_4 & 0 \\ \alpha_4 & 0 & 0 \end{pmatrix} \tag{21}$$

### *2.2. Aerodynamics*

Adopting a segregated-solver formulation of the aeroelastic computational routine allowed modularity in the aerodynamic solver. The use of simple analytical theories and semi-empirical models to compute the aerodynamic loading for zeroth-order aeroelastic prediction was intented in this work. To this end, two aerodynamic methods were implemented in MATLAB for interface-less computation, whilst computation using external aerodynamic solvers was investigated through interfacing the aeroelastic computational framework in MATLAB with a public domain version of SHABP Mk IV.

The aerodynamic methods that were made native to the computational framework included shock-expansion (SE) theory applied over chordwise strips and local piston theory (Zhang et al., 2009; McNamara et al., 2010). The methods were applied with SE providing the mean steady loading, and local piston theory (LPT) providing the perturbation loading due to plate motion; this is referred to as SE/LPT. The LPT routine was also used to provide the perturbation loading when the mean steady load was computed by SHABP; this is referred to as SHABP/LPT. In this way, the aeroelastic framework was developed to be modular with steady aerodynamic methods.

The familiar oblique-shock relations utilized in shock-expansion theory are not repeated here. The formulation of local piston theory, however, is outlined. The mean steady flow conditions as determined from the steady aerodynamic methods (shock-expansion theory or SHABP) were used as the cylinder reference conditions in LPT, and the perturbation downwash relative to the mean steady state was utilized in the LPT routine. The perturbation downwash $w_p$ was found by:

$$w_p = V_m \frac{\partial z_p}{\partial x} + \frac{\partial z_p}{\partial t} \tag{22}$$

where $V_m$ is the local mean-steady flow velocity, $z_p$ is the perturbation displacement, and $x$ is the chordwise coordinate. The perturbation pressure $P_p$ modeled by 3$^{\text{rd}}$-order LPT was given by:

$$\frac{P_p}{P_m} = 1 + \gamma \left[ c_1 \left( \frac{w_p}{a_m} \right) + c_2 \left( \frac{w_p}{a_m} \right)^2 + c_3 \left( \frac{w_p}{a_m} \right)^3 \right] \tag{23}$$

where $P_m$ is the local mean-steady pressure, $\gamma$ is the specific heat ratio, $a_m$ is the local mean-steady speed of sound, and where the piston-theory coefficients were modeled using Donov's (Donov, 1956) 3$^{\text{rd}}$-order theory:

$$c_1 = \frac{M}{m} \tag{24}$$

$$c_2 = \frac{M^4 (\gamma + 1) - 4m^2}{4m^4} \tag{25}$$

$$c_3 = \frac{1}{6Mm^7} \left( a_1 M^8 + a_2 M^6 + a_3 M^4 + a_4 M^2 + a_5 \right) \tag{26}$$

$$m = \sqrt{M^2 - 1} \tag{27}$$

where $M$ is the local mean-steady Mach number, and where the coefficients $a_1$ through $a_5$ are dependent on whether the flow is locally undergoing compression or expansion, with the coefficients being defined in Table 1. Donov's coefficients are derived from a method of characteristics analysis, and provide extension to higher-order terms relative to the coefficients of Van Dyke (Van Dyke, 1952), which in themselves are truer approximations to the flow physics than the coefficients of Lighthill (Lighthill, 1953).

Table 1: Third-order piston theory contribution coefficients from Donov (1956).

| Flow behaviour | $a_1$ | $a_2$ | $a_3$ | $a_4$ | $a_5$ |
|---|---|---|---|---|---|
| Expansion | $(\gamma+1)/2$ | $\left(2\gamma^2-7\gamma-5\right)/2$ | $5(\gamma+1)$ | $-6$ | 4 |
| Compression | $3(\gamma+1)^2/16$ | $\left(3\gamma^2-12\gamma-7\right)/4$ | $9(\gamma+1)/2$ | $-6$ | 4 |

The aerodynamic loading computed away from structural nodes was interpolated to structural nodes as required.

## 3. Results and Discussion

The zeroth-order flutter prediction capability of the computational aeroelastic framework developed in MATLAB was tested against publicly available experimental data. Two particular series of experiments considered were the flutter test of the Torii-Matsuzaki plate (Torii, 2012; Matsuzaki, 2011) and the series of flutter tests of Tuovila and McCarty (1955). In both cases, the supersonic flutter of swept cantilevered plates was determined by wind-tunnel testing. The Torii-Matsuzaki case is particularly valuable in providing an estimation of the damping and frequencies at condition below flutter (Torii, 2012) and in showing qualitatively the onset of hard flutter (Matsuzaki, 2011). The Tuovila and McCarty (1955) series of tests provide data on the variation of the flutter point with plate sweep and Mach number. The geometry of the reference cases is defined in Fig. 1(a) and Table 2.

The structural solver was validated against NASTRAN; the natural frequencies of the Torii-Matsuzaki plate were predicted to within 1% of the NASTRAN values when using equivalent models and good agreement was obtained with reference values, as shown in Table 3. The mode shapes are depicted in Fig. 2.

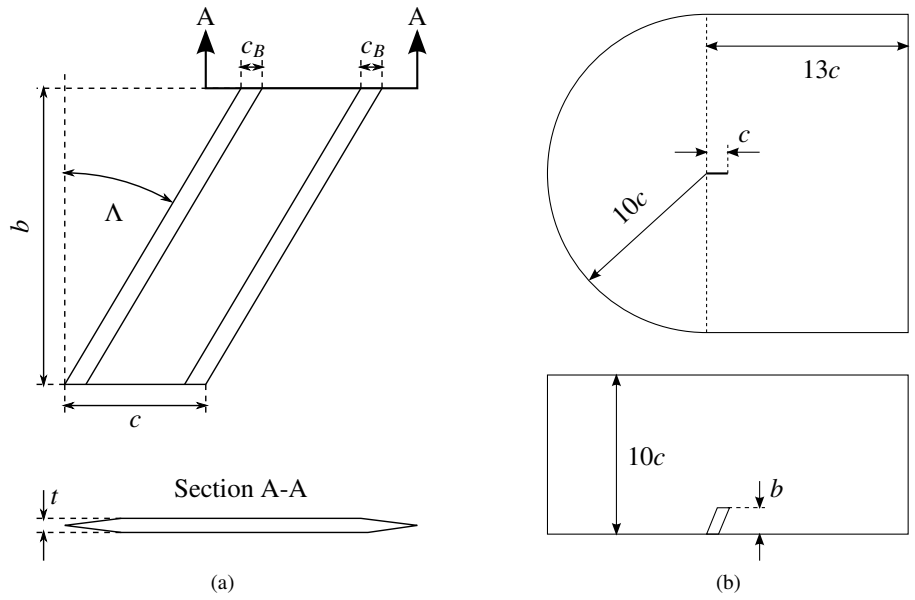


Figure 1: Geometry of: (a) a generic untapered, swept cantilevered plate (b) the computational domain for the CFD analysis of the Torii-Matsuzaki plate.

Table 2: Geometries of the reference experimental models, with symbols defined in Fig. 1.

| Reference | Model | $\Lambda$ (°) | $c$ (mm) | $c_B$ (mm) | $b$ (mm) |
|---|---|---|---|---|---|
| Tuovila and McCarty (1955) | 5151 | 15 | 52.6 | 6.58 | 140 |
| Tuovila and McCarty (1955) | 4301 | 30 | 58.7 | 7.34 | 122 |
| Tuovila and McCarty (1955) | 3451 | 45 | 71.8 | 8.98 | 99.0 |
| Matsuzaki (2011) | N/A | 30 | 100 | 15.0 | 220 |

Table 3: Structural frequencies of the Torii-Matsuzaki plate (Meijer, 2014).

| | Natural frequency, $f$ (Hz) | | |
|---|---|---|---|
| Analysis Method | Mode 1 | Mode 2 | Mode 3 |
| Experimental (Torii, 2012) | 27.2 | 142.0 | 192.3 |
| MATLAB | 26.4 | 147.7 | 192.4 |
| NASTRAN | 26.6 | 148.5 | 195.0 |

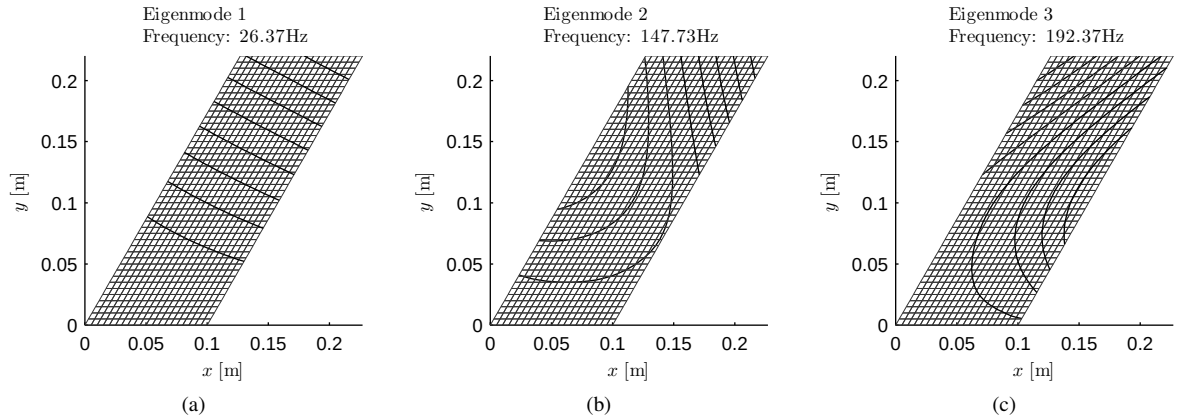


Figure 2: Natural mode shapes and frequencies for the Torii-Matsuzaki plate: (a) first bending (b) first torsion-bending (b) second torsion-bending.

In this work, the Torii-Matsuzaki plate was also modeled using the Edge 5.2.0 CFD code. Coupled modal solutions were run on an unstructured mesh of 1.43 million tetrahedral elements on the domain defined in Fig. 1(b) after an inital mesh independence study. Implicit time-marching with a physical time-step $\Delta t = 1.306\text{x}10^{-4}$s was used; this was chosen by applying Eq. (13) to the sixth structural mode, a conservative choice (Katona et al., 1977) resulting in few inner iterations of the strongly-coupled system being required. The chosen time-step resulted in a resolution of approximately 70 steps per cycle at the flutter frequency. The same time-step was used in both the MATLAB direct integration and in the CFD solution. Euler solutions were obtained at Mach 2.51 for a sweep of dynamic pressures. The resulting structural responses from small initial disturbances were analyzed to determine the flutter dynamic pressure $q_F$ and flutter frequency $f_F$. The aeroelastic analysis in Edge was used as a comparison point for accuracy and computational cost of flutter prediction for the developed zeroth-order flutter prediction framework in MATLAB. The results of the computational analyses of the Torii-Matsuzaki plate are given in Table 4, with the approximate computational time required at each flight condition given in Table 5.

Good agreement with the experimental flutter dynamic pressure was obtained by all the computational methods, to within 10% of the experimental value. The methods in the zeroth-order framework are seen to give unconservative predictions of the flutter dynamic pressure, whilst the Euler computation in Edge gives a conservative result.

Table 4: Flutter conditions of the Torii-Matsuzaki plate (Meijer, 2014).

| Analysis Method | $q_F$ (kPa) | %Error in $q_F$ | $f_F$ (Hz) |
|---|---|---|---|
| Experimental (Torii, 2012) | 113.5 | N/A | N/A |
| Edge 5.2.0 | 108.3 | -4.6% | 107 |
| SE/LPT (nonlinear) | 120.8 | +6.4% | 112 |
| SE/LPT (linearized) | 124.5 | +9.7% | 108 |
| SHABP/LPT (linearized) | 117.9 | +3.9% | 108 |

Table 5: Approximate time required for determination of aeroelastic modal parameters at a flight condition (Meijer, 2014).

| Analysis Method | Time* | Remarks |
|---|---|---|
| Edge 5.2.0 | 7 hours | 1500 time steps |
| SE/LPT (nonlinear) | 9 hours | 1500 time steps |
| SE/LPT (linearized) | 3 minutes | 20 x 44 panels |
| SHABP/LPT (linearized) | 5 minutes | 10 x 26 panels |

*8-core AMD FX-8150 3.6GHz processor, 8GB RAM, and Microsoft Windows 7.

The direct integration of the full-order model in MATLAB (involving matrix inversion) is seen to be computationally more expensive than the numerical scheme of Edge. Good agreement in the frequency trends between the full-order and the linearized modal models using SE/LPT is observed in Fig. 3, with fair agreement of the SE/LPT trends with those predicted in Edge. This suggests that the aeroelastic trends may be predicted with good confidence using the linearized modal formulation of SE/LPT at a fraction of the computational cost required ($\approx$ 140 times less) for higher-fidelity analysis.

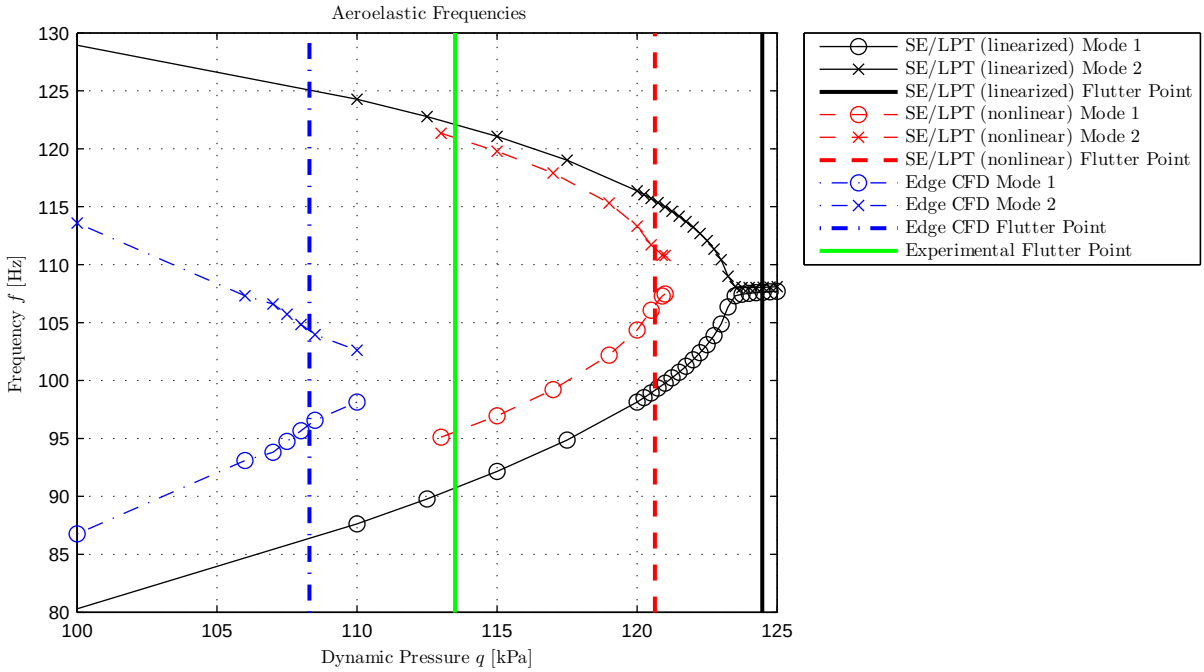


Figure 3: Comparison of the flutter predictions for the Torii-Matsuzaki plate (Meijer, 2014).

The closest agreement to experiment was given by the use of SHABP within the LPT framework; however, the computation required more time than the MATLAB-native SE/LPT analysis, likely due to read/write operations associated with the execution of SHABP. The vast majority of the computation time of the SE/LPT implementation was associated with the implementation of shock-expansion theory. Room exists for optimization of the implementation; the framework which was developed in MATLAB could be implemented in existing software or in other computational languages.

The variation of the aeroelastic modal parameters of the Torii-Matsuzaki plate with dynamic pressure predicted by SE/LPT is shown in Fig. 4.

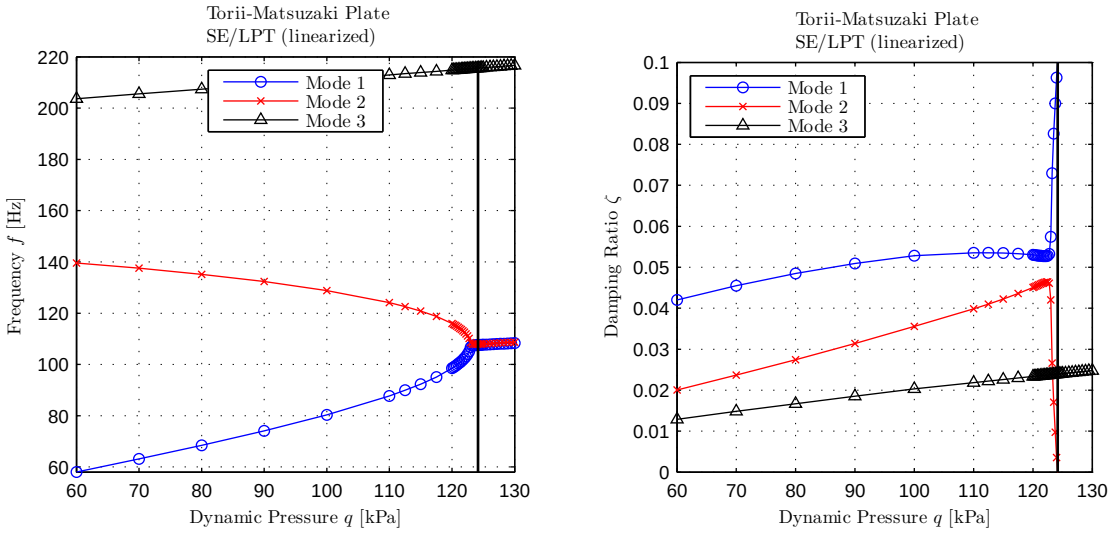


(a) (b)

Figure 4: Aeroelastic modal parameter variation predicted by shock-expansion/local piston theory (Meijer, 2014) for the Torii-Matsuzaki plate: (a) frequencies (b) damping ratios.

The very sharp decrease in damping of the pitch-dominated first torsion-bending mode (Mode 2, Fig. 4(b)) near flutter shows that the hard flutter of the Torii-Matsuzaki plate, as experienced in wind-tunnel testing (Matsuzaki, 2011), is modeled. This is significant in showing that the linearized modal formulation can correctly predict behaviour of the damping as flutter is approached.

The ability to rapidly numerically investigate the flutter behaviour of the plate would be valuable in the planning of flutter wind-tunnel tests. The near-linear behaviour of the Zimmerman-Weissenburger flutter margin seen in Fig. 5 for the linearized modal formulation allows the flutter point to be accurately extrapolated from a small number of computations below the flutter speed. This further reduces the computational effort required in estimating the flutter boundary.

The results of the SE/LPT analysis in MATLAB were further compared to the experiments of Tuovila and McCarty (1955) to determine the fidelity of the framework for variations in plate geometry. The reference flutter conditions are given in Table 6. The tests of Tuovila and McCarty have previously served as validation cases for aeroelastic predictions — the results from SE/LPT in the present work are compared to the predictions from ZONA7 and ZONA7U (Chen et al., 1999), conical flow and piston theory (Xianxin, 1983), and second-order classical piston theory (Morgan et al., 1958) where available in Figs. 6 – 8. No attempt is made to benchmark the computation times of the methods, as the ZONA7 code was not available to the authors.

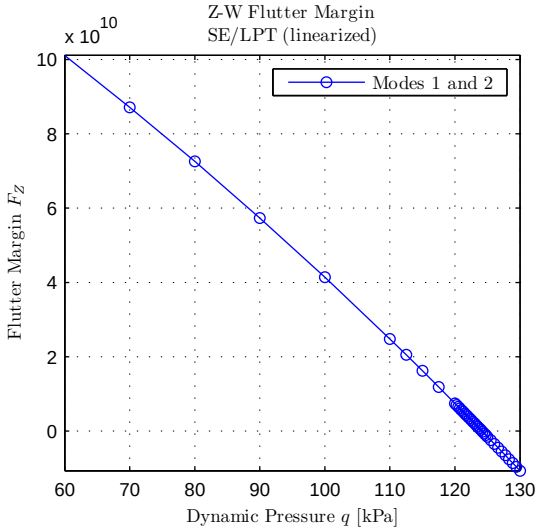


Figure 5: Zimmerman-Weissenburger flutter margin predicted by shock-expansion/local piston theory (Meijer, 2014) for the Torii-Matsuzaki plate.

Table 6: Experimental flutter conditions of the Tuovila and McCarty (1955) models.

| | Model 5151 | | Model 4301 | | Model 3451 | |
|---|---|---|---|---|---|---|
| $M_\infty$ | $q_F$ (kPa) | $f_F$ (Hz) | $q_F$ (kPa) | $f_F$ (Hz) | $q_F$ (kPa) | $f_F$ (Hz) |
| 1.3 | 19.22 | 102 | 17.26 | 94 | 24.71 | 180 |
| 2.0 | 35.81 | 134 | 29.06 | 142 | 29.73 | 148 |
| 3.0 | 91.74 | 146 | 66.10 | 158 | 60.18 | 170 |

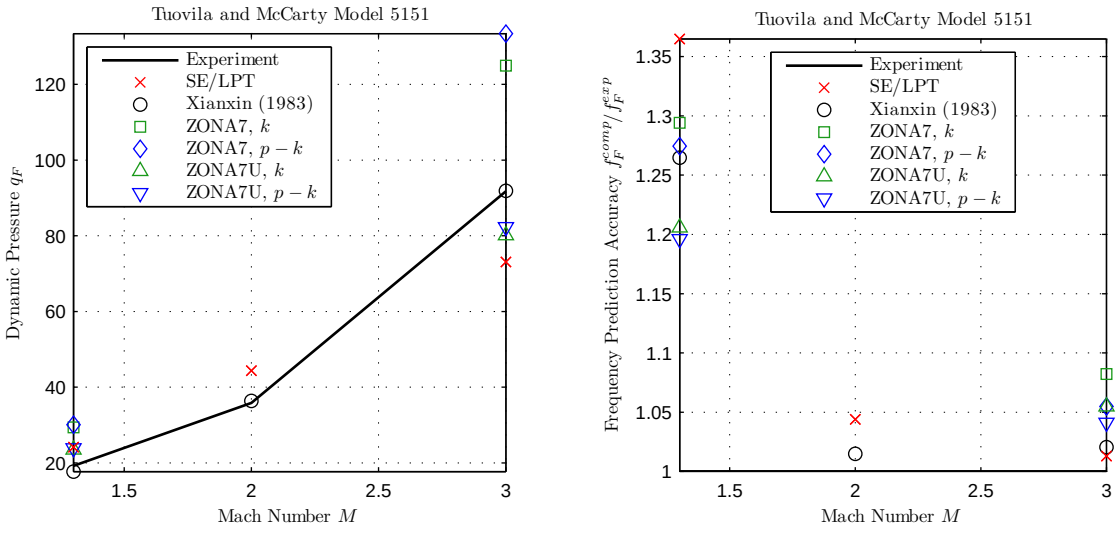


(a) (b)

Figure 6: Comparison of predicted and expermental flutter conditions of Tuovila and McCarty (1955) Model 5151: (a) flutter dynamic pressure, (b) flutter frequency. ZONA7 results quoted from Chen et al. (1999).

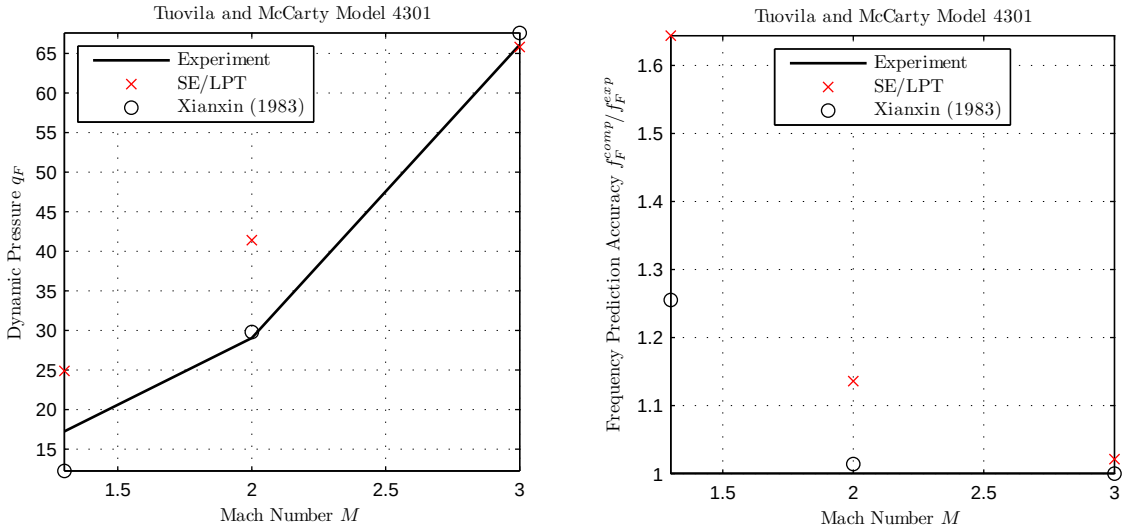


(a) (b)

Figure 7: Comparison of predicted and expermental flutter conditions of Tuovila and McCarty (1955) Model 4301: (a) flutter dynamic pressure, (b) flutter frequency. ZONA7 results quoted from Chen et al. (1999).

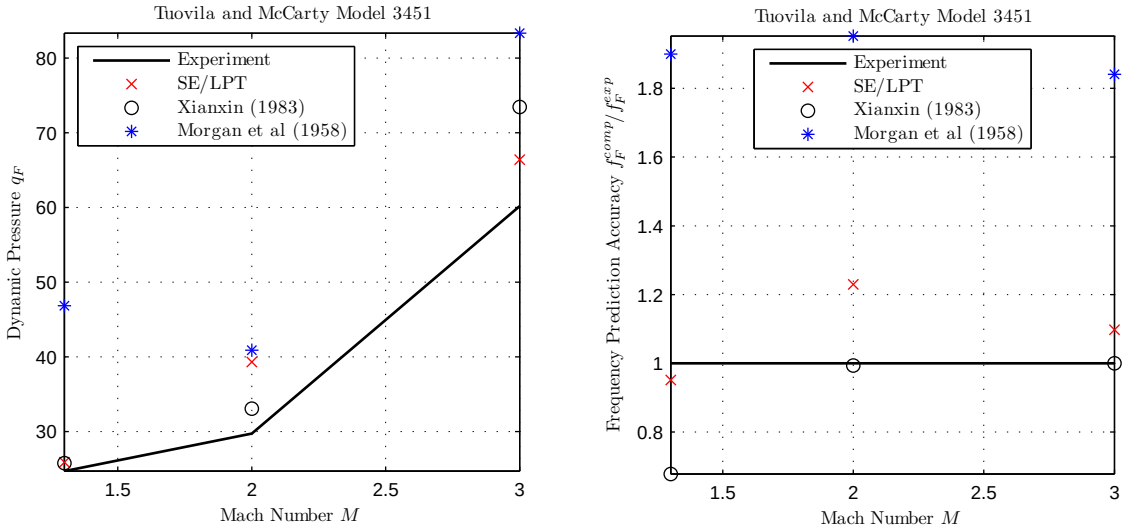


(a) (b)

Figure 8: Comparison of predicted and expermental flutter conditions of Tuovila and McCarty (1955) Model 3451: (a) flutter dynamic pressure, (b) flutter frequency. ZONA7 results quoted from Chen et al. (1999).

The trend of the flutter dynamic pressure variation with Mach number is generally well reproduced by the linearized modal formulation of SE/LPT for the various models (subfigures (a) in Figs. 6 – 8). Generally superior agreement is obtained by the conical flow and piston-theory approach of Xianxin (1983); this is expected, as proper treatment is made of the zones of influence over the finite wing. The dynamic pressure prediction of SE/LPT is found to be superior to that of ZONA7 for the considered geometry and Mach numbers, whilst being similar to ZONA7U (which accounts for thickness effects). The clear superiority over the second-order classical piston theory computation

of Morgan et al. (1958) emphasizes the limitations of classical piston theory.

Consideration of the prediction of the flutter frequency (subfigures (b) in Figs. 6 – 8) gives similar conclusions, with the exception that the frequency is universally over-predicted at Mach 1.3, and with SE/LPT yielding better prediction of the frequency than the ZONA codes for the given geometry at Mach 3.

## 4. Conclusions

The developed zeroth-order flutter prediction framework utilizing a native implementation of SE/LPT in MATLAB was shown to be suitable for aeroelastic prediction of cantilevered plates. Good accuracy of flutter prediction ($q_F$ within 10% of experimental values) was obtained at significantly reduced computation times ($\approx$ 140 times shorter) relative to unsteady Euler computations. Scope for optimized and extended implementation remains. A preliminary extension of the implementation to coupling with a public domain version of SHABP Mk IV was successfully accomplished. The SHABP/LPT implementation also gave good accuracy of flutter prediction at reduced computational cost ($q_F$ within 5%, $\approx$ 80 times shorter computation than CFD).

The public domain version of SHABP Mk IV is limited in the extent of discretization that is possible (the number of panels is limited). The merit of the use of SHABP lies in the various appropriate approximate aerodynamic methods available for flow computation over an arbitrary body configuration. The current work suggests that extension of the capabilities of the code and improved interfacing with the developed zeroth-order framework could yield a valuable tool for computationally inexpensive aeroelastic prediction for complex configurations at high supersonic to hypersonic speeds. The use of local piston theory in the framework facilitates modularity in the quasi-steady aerodynamic solver, and thus the framework could also be extended to other computational routines.

The success of approximate aerodynamic methods in predicting the flutter trends and behaviour such as hard flutter of cantilevered plate-like structures has been reiterated, with good agreement to experiment demonstrated for various geometries. The value of zeroth-order modeling in reproducing trends at significantly reduced computational cost has been emphasized as a complement and input to higher-fidelity analysis.

## Acknowledgements

The financial support of this work through the Fluxion grant of ARMSCOR and the use of the Edge CFD code through the CSIR of South Africa is gratefully acknowledged.

## References

Chen, P., Sarhaddi, D., Liu, D., Striz, A., 1999. Development of the aerodynamic/aeroservoelastic modules in ASTROS, Vol. 3: ZAERO applications manual. ZONA 99-11C, ZONA Technology, Inc, Scottsdale, AZ.

Dimitriadis, G., 2001. Investigation of nonlinear aeroelastic systems. Ph.D. thesis, University of Manchester.

Donov, A., 1956. A flat wing with sharp edges in a supersonic stream. NACA TM-1394.

Ferreira, A., 2008. MATLAB Codes for Finite Element Analysis: Solids and Structures. Springer.

Gentry, A., Smyth, D., Oliver, W., 1973. The Mark IV Supersonic-Hypersonic Arbitrary-Body Program, Vol. I: Users Manual. AFFDL TR-73-159.

Katona, M., Thompson, R., Smith, J., 1977. Efficiency study of implicit and explicit time integration operators for finite element applications. Cel-tr-856, Civil Engineering Laboratory, Port Hueneme, CA.

Lighthill, M., 1953. Oscillating airfoils at high Mach numbers. Journal of the Aeronautical Sciences 20 (6), 402–406.

Livne, E., 2003. Future of airplane aeroelasticity. Journal of Aircraft 40 (6), 1066–1092.

Matsuzaki, Y., 2011. An Overview of Flutter Prediction in Tests Based on Stability Criteria in Discrete-Time Domain. International Journal of Aeronautical and Space Sciences 12 (4), 305–317.

McNamara, J., Crowell, A., Friedmann, P., Glaz, B., Gogulapati, A., 2010. Approximate modeling of unsteady aerodynamics for hypersonic aeroelasticity. Journal of Aircraft 47 (6), 1932–1945.

McNamara, J., Friedmann, P., 2007. Flutter boundary identification for time-domain computational aeroelasticity. AIAA Journal 45 (7), 1546–1555.

McNamara, J., Friedmann, P., 2011. Aeroelastic and aerothermoelastic analysis in hypersonic flow: past, present, and future. AIAA Journal 49 (6), 1089–1122.

Meijer, M.-C., 2014. Aeroelastic prediction for missile fins in supersonic flows. In: 29th International Congress of the Aeronautical Sciences. St. Petersburg, Russia.

Morgan, H., Huckel, V., Runyan, H., 1958. Procedure for calculating flutter at high supersonic speed including camber deflections, and comparison with experimental results. NACA TN-4335.

Rodden, W., Farkas, E., Malcom, H., Kliszewski, A., 1962a. Aerodynamic Influence Coefficients from Piston Theory: Analytical Development and Computational Procedure. Report No. TDR-169(3230-11)TN-2, Aerospace Corporation, El Segundo, CA.

Rodden, W., Farkas, E., Malcom, H., Kliszewski, A., 1962b. Aerodynamic Influence Coefficients from Supersonic Strip Theory: Analytical Development and Computational Procedure. Report No. TDR-169(3230-11)TN-1, Aerospace Corporation, El Segundo, CA.

Torii, H., 2012. The extension of discrete-time flutter margin. In: 28th International Congress of the Aeronautical Sciences. Brisbane, Australia.

Tuovila, W., McCarty, J., 1955. Experimental Flutter Results for Cantilever-Wing Models at Mach Numbers up to 3.0. NACA RM L55E11.

Van Dyke, M., 1952. A study of second-order supersonic flow theory. NACA Report 1081.

Xianxin, W., 1983. A new method for calculating supersonic unsteady aerodynamic forces and its application. Acta Aeronautica et Astronautica Sinica 4 (3), 9–18.

Yurkovich, R., 2003. Status of unsteady aerodynamic prediction for flutter of high-performance aircraft. Journal of Aircraft 40 (5), 832–842.

Zhang, W.-W., Ye, Z.-Y., Zhang, C.-A., Liu, F., 2009. Supersonic flutter analysis based on a local piston theory. AIAA Journal 47 (10), 2321–2328.